AIAA JOURNAL
Vol. 38, No. 11, November 2000

Numerical Simulation of a Mach 1.92 Turbulent Jet and Its Sound Field

J. B. Freund*
University of California, Los Angeles, Los Angeles, California 90095
and
S. K. Lele† and P. Moin‡
Stanford University, Stanford, California 94305

A perfectly expanded turbulent Mach 1.92 jet is simulated by direct numerical solution of the compressible Navier–Stokes equations in a computational domain that includes the near acoustic field. In place of a nozzle, turbulent inflow data were generated in a separate streamwise periodic jet simulation. Reynolds stresses, two-point correlations, and turbulent energy spectra are computed and discussed. The sound field is highly directional and dominated by Mach waves as are commonly observed experimentally. Analysis of the sound using weak-shock theory shows that nonlinear effects are significant away from the jet but that linear theory is sufficient to estimate near-field sound pressure levels. Although no attempt was made to match any particular experiment in detail, sound pressure levels are compared with experimental data at similar flow conditions and are found to agree in general with jets at similar convective Mach numbers.

Nomenclature

a	=	speed of sound
D	=	jet diameter
ℓ	=	a correlation length scale
M_c	=	convective Mach number
p	=	pressure
r_o	=	jet nozzle radius
s	=	ray coordinate
T	=	fluid temperature
U	=	fluid velocity
(v_x, v_r, v_θ)	=	fluid velocities
(x, r, θ)	=	cylindrical coordinate
μ	=	viscosity
ρ	=	fluid density

Subscripts

j	=	jet exit conditions
∞	=	ambient condition

Superscripts

$'$	=	Reynolds averaged perturbation
$''$	=	Favre averaged perturbation

I. Introduction

THE reduction of acoustic emissions is one of the key technological challenges facing proposed high-speed civilian transports. Meeting airport noise regulations, which in some cases are already restricting the use of present-day subsonic aircraft, will be nearly impossible without a substantial technological breakthrough, especially on aircraft where the jet exhaust velocity is supersonic. A firm understanding of the physics is necessary to guide such progress.

Presented as Paper 98-2291 at the AIAA/CEAS 4th Aeroacoustics Conference, Toulouse, France, 2–4 June 1998; received 8 May 1999; revision received 20 September 1999; accepted for publication 10 April 2000.

*Assistant Professor, Mechanical and Aerospace Engineering. Member AIAA.
†Associate Professor, Mechanical Engineering and Department of Aeronautics and Astronautics. Member AIAA.
‡Franklin and Caroline Johnson Professor, Mechanical Engineering; also Senior Staff Scientist, NASA Ames Research Center, Moffett Field, CA 95035. Associate Fellow AIAA.

In the present study we focus on a perfectly expanded supersonic round jet issuing into a quiescent ambient environment. It has been observed experimentally that the acoustic radiation from such jets is dominated by Mach waves (see reviews by Tam[1,2]). Turbulent structures traveling at supersonic speeds within the jet are generally thought to be responsible for this, and they have been successfully modeled by Tam and Burton[3] as linear stability modes. In a jet excited at a particular frequency, Tam and Burton showed nearly perfect agreement between the predicted and measured sound fields to within a constant that was indeterminable by linear theory. To determine the bounds of applicability of linear theory and examine the jet in full detail it is, however, necessary to include nonlinear effects.

In this paper, we present a direct numerical simulation of a supersonic turbulent jet and its sound field and show some fundamental results obtained from the simulation database. Although this approach is too computationally intensive to be employed presently as a predictive tool, it is uniquely capable of providing detailed simultaneous information of both the flowfields and sound fields and is, therefore, invaluable for studying jet noise and examining jet noise models. The flow parameters and simulation techniques are introduced in Sec. II. Section III documents the jet turbulence. Sound field results and techniques for extending the computation into the far-acoustic field are discussed in Sec. IV, which also compares sound pressure levels to experimental data. Though a realistic turbulent jet has been simulated, it was not possible to conduct a first principles computation while at the same time matching the flow parameters of any particular experiment. Thus, a precise point-to-point comparison with an experiment is not possible. Nevertheless, agreement with similar experiments is favorable. Conclusions are stated in Sec. V.

II. Numerical Simulations

A. Flow Parameters

The subject of the present study is a Mach 1.92 (U_j/a_j) round jet exiting into a quiescent infinite domain. The jet is heated with exit temperature ratio $T_j/T_\infty = 1.12$. Based on this, the isentropic convective Mach number[4] for the jet shear layers was $M_c = 0.99$. The Reynolds number was

$$Re = \rho_j U_j D_j / \mu_j = 2000 \tag{1}$$

and the Prandtl number was 0.7. This Reynolds number is low compared to that in the available experimental data; however, comparing different experiments at different Reynolds numbers but similar

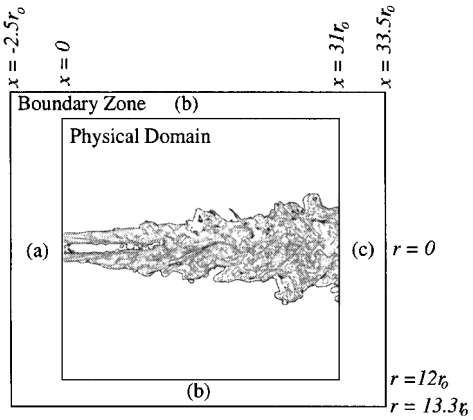

Fig. 1 Computational domain schematic showing the physical domain and the boundary zones: a) inflow zone, b) far-field zone, and c) outflow zone.

Mach numbers shows that the acoustic radiation's peak Strouhal number is independent of Reynolds number (though jets at Reynolds numbers as low as 2000 have not been studied in this way).[2] One effect of increasing the Reynolds number is to broaden the spectrum, though the spectral makeup of the noise is complex and not independent of the radiation direction. Some degree of Reynolds number insensitivity is also in accord with the theory of Tam and Burton[3] because the linear stability modes used as sources in their analysis are independent of viscosity for the Reynolds numbers considered. The incompressible results of Morris[5] suggest that viscosity plays only a very small role in jet stability for Reynolds numbers above 1000, though it has been shown that the role of viscosity increases with increasing compressibility.[6] Nevertheless, we expect at most a small influence of viscosity on the dominant acoustic modes at the present Reynolds number. On the other hand, details of the development of the flow turbulence is likely to be somewhat Reynolds number dependent.

B. Equations and Numerical Method

The computational domain is shown schematically in Fig. 1. In this domain, the fully compressible Navier–Stokes equations were solved in cylindrical coordinates and without modeling assumptions. The functional dependence of viscosity on temperature was specified with Sutherland's law and a perfect gas state equation with $\gamma = 1.4$ closed the equations. The basic numerical method was essentially the same as used by Freund et al.[7] Sixth-order compact finite differences were used in the axial and radial directions x and r, and Fourier spectral methods were used in the azimuthal θ direction. Time advancement was by a fourth-order Runge–Kutta algorithm. At the coordinate singularity, $r = 0$, the equations were solved in Cartesian coordinates. Near $r = 0$, the geometry of the cylindrical mesh causes the θ-mesh spacing to become very small, and this imposes a severe time-step restriction. To alleviate this, higher Fourier modes in θ were systematically omitted in such a way that the effective resolution in θ was nearly constant with radial location. A similar code was used to study a Mach 0.9 jet and showed excellent quantitative agreement with a corresponding experiment in that case.[8]

The present computational mesh had $640 \times 270 \times 128$ ($= 22 \times 10^6$) points in the axial, radial, and azimuthal directions, respectively. Mesh points were compressed in the radial direction near $r = r_o$, where r_o is the nozzle radius, and in the axial direction near the end of the potential core $x \approx 11r_o$. The minimum and maximum spacings were $0.019r_o$ and $0.11r_o$ in the r direction and $0.046r_o$ and $0.11r_o$ in the x direction. These were arrived at iteratively by careful examination of the resolution needs of different regions and mesh refinement studies. The point-to-point change in mesh spacing was less than 2% in each direction. The physical portion of the computational domain extended from $x = 0$ to $31r_o$ in the axial direction and to $12r_o$ in the radial direction. The numerical timestep was determined so that the Courant–Friedrichs–Lewy number remained near unity. A typical timestep was $\Delta t = 0.006r_o/a_\infty$.

C. Boundary Conditions

Unless perturbed in some significant way, a $Re = 2000$ jet will have laminar shear layers that are stabilized by their viscous spreading. Thus, in this study a novel technique was used to excite the shear layers at the inflow boundary to give the jet some characteristics of a flow at a higher Reynolds number. It was also deemed computationally too expensive to both simulate a nozzle and still resolve all relevant turbulent scales in the jet. To accomplish these joint objectives, data from a turbulent streamwise periodic jet simulation[7] were fed into the present calculation. A special zonal boundary condition was developed to facilitate this while at the same time minimizing spurious reflections.[9] In the inflow zone (zone a in Fig. 1), terms were added to the equations that pass the incoming turbulence into the physical domain undamped, but strongly damp the outgoing waves. The simulations used to generate the inflow turbulence had a streamwise period of $21r_o$, which was sufficient to decorrelate the turbulence in the streamwise direction.[7] It was passed into the spatial computation at $M_c = 0.99$. In these auxiliary computations, the turbulence was initialized with broadbanded, randomly phased velocity disturbances and then allowed to develop naturally. Full details of the inflow turbulence are provided elsewhere.[7,10] The specific flow parameters for the present study were selected due to the availability of this inflow data. In the present spatially developing simulation, the amplitudes of the two-dimensional spectral components of the incoming turbulence were randomly jittered by up to 5% of their amplitude to break the $21r_o$ periodicity. To increase the statistical sample still further and verify that results did not depend on the particular data fed into the domain, two distinct fields from Freund et al.[7] were used in the course of the simulations. Both fields had a momentum thickness of $\delta_m = 0.10r_o$. The streamwise periodic shear layers grew to this thickness before being feed into the present computation.

In the far-field and outflow boundary zones (Figs. 1b and 1c), convection and damping terms, as discussed by Freund,[9] were added to the equations to absorb outgoing disturbances with minimal reflections. The mean flow for damping outgoing disturbances was estimated by extrapolating data from the interior of the domain. The inflow (Fig. 1a) and outflow (Fig. 1c) zones were both $2.5r_o$ wide, and the far-field zone (Fig. 1b) was $1.3r_o$ wide.

III. Turbulence Results

After achieving statistical steady state, the simulations were run for approximately $T_{\text{sim}} = 500r_o/a_\infty$ time units, where a_∞ is the ambient speed of sound. This corresponds to the time required for an acoustic wave to propagate the length of the physical domain 15 times and was also sufficient to converge most turbulence statistics. Over a hundred samples of the flow were used to calculate the statistics.

A. Mean Flow

Figure 2 shows the mean streamwise velocity, radial velocity, and density. The velocities are normalized by U_j, the jet exit centerline velocity. The mean axial velocity (Fig. 2a) evolves from a rounded top-hat shape near the inflow boundary to a Gaussian shape after the potential core closes at around $x/r_o = 11$. Note that the effective nozzle diameter will vary slightly from $2r_o$ depending on where its location is taken to be. The streamwise periodic flow used to force the inflow of this simulation was initialized with a hyperbolic tangent profile centered at r_o with momentum thickness 0.08 (Ref. 10).

The radial mean velocity (Fig. 2b) is naturally much smaller than the axial flow. It is positive near the domain centerline (except at $x \approx 0$) and becomes negative away from the jet. At large r it decays roughly like $1/r$, indicative of entrainment induced potential flow appropriate for the irrotational region. There are suspicious wiggles in the large r profiles near the inflow and outflow that are believed to be due to the influence of boundary conditions. The reader is reminded that the radial velocity is very small and these minor deviations are not likely to adversely affect the solution on the whole. There is also anomalous behavior at small r near the inflow. This is due to a very weak array of compression/rarefaction waves in the potential core of the jet. The compressions are sufficiently weak to remain well resolved on the computational mesh.

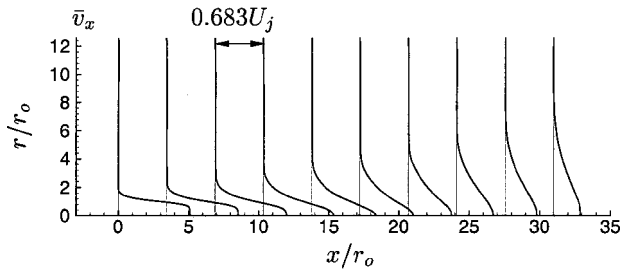

a) Axial velocity

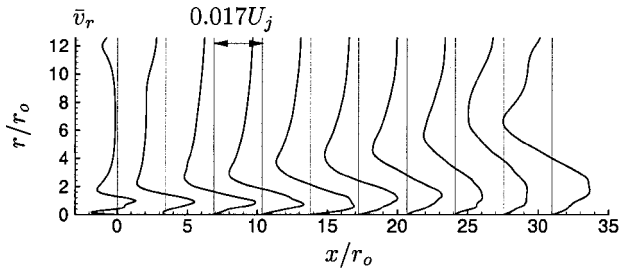

b) Radial velocity

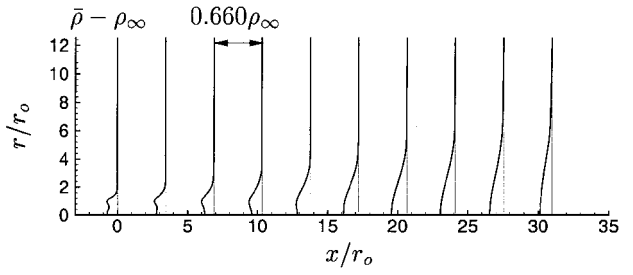

c) Density

Fig. 2 Mean flow.

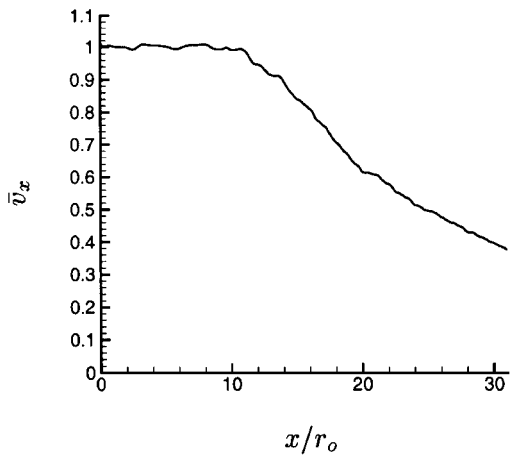

Fig. 3 Mean axial velocity at $r = 0$.

Mean density profiles are shown in Fig. 2c normalized by the ambient density. There is again peculiar behavior near the inflow associated with the compression waves, and there is also evidence of viscous heating in the mixing layer prior to the potential core closure. The centerline streamwise velocity is plotted in Fig. 3 and the point where the potential core closes is clearly evident.

B. Reynolds Stresses

Reynolds stresses are plotted in Fig. 4 and Favre averaged Reynolds stresses are plotted in Fig. 5. Reynolds averaged stresses are typically measured in experiments, but modeling of compressible turbulence is typically done with Favre averages. There is clearly very little difference between the two at this Mach number, and for the present we discuss them interchangeably.

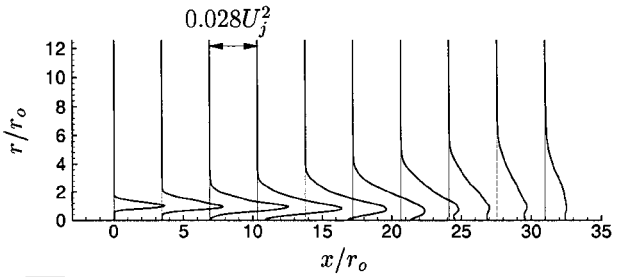

a) $\overline{v_x' v_x'}$

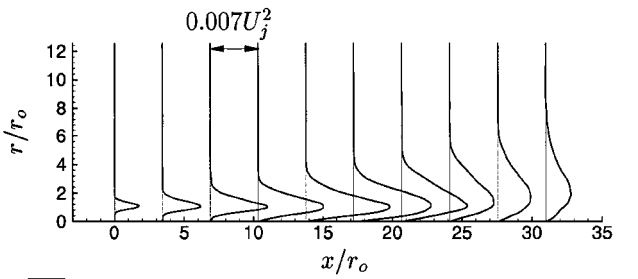

b) $\overline{v_x' v_r'}$

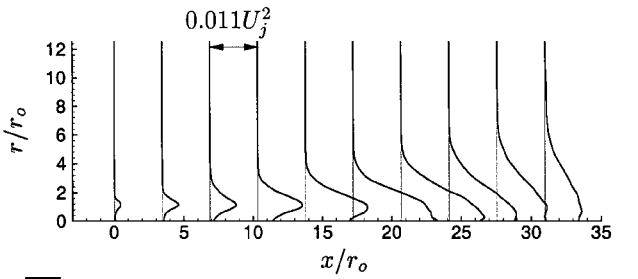

c) $\overline{v_r' v_r'}$

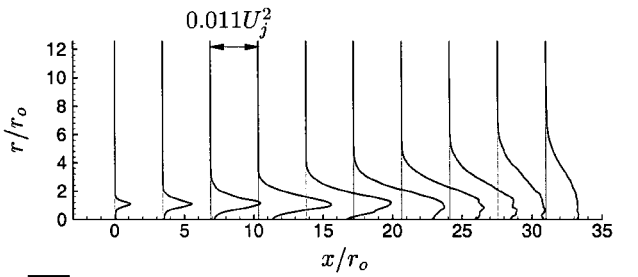

d) $\overline{v_\theta' v_\theta'}$

Fig. 4 Reynolds stresses.

Examining the results, we see that, before the potential core closes, axial normal stress is peaked in the middle of the jet shear layer around $r = r_o$. This peak at $r = r_o$ persists after the potential core closes and only completely disappears by the final profile plotted. Crow and Champagne[11] showed a similar persistence of a peak at $r = r_o$. Clearly, a self-similar state is not achieved in the present simulations. The axial normal intensity and Reynolds shear stress both peak at approximately the same position where the potential core closes. The radial and azimuthal normal stresses peak slightly later, but also in the vicinity of the potential core closing. We shall see later that most of the acoustic radiation comes from this same highly turbulent region of the flow.

C. Length Scales and Two-Point Correlations

We estimate a turbulence length scale in a particular direction by the 50% correlation distance of the velocity component in that direction. Thus, if

$$\overline{v_x'(x_o - x_l)v_x'(x_o)} = 0.5\overline{v_x'(x_o)v_x'(x_o)} \tag{2}$$

$$\overline{v_x'(x_o + x_r)v_x'(x_o)} = 0.5\overline{v_x'(x_o)v_x'(x_o)} \tag{3}$$

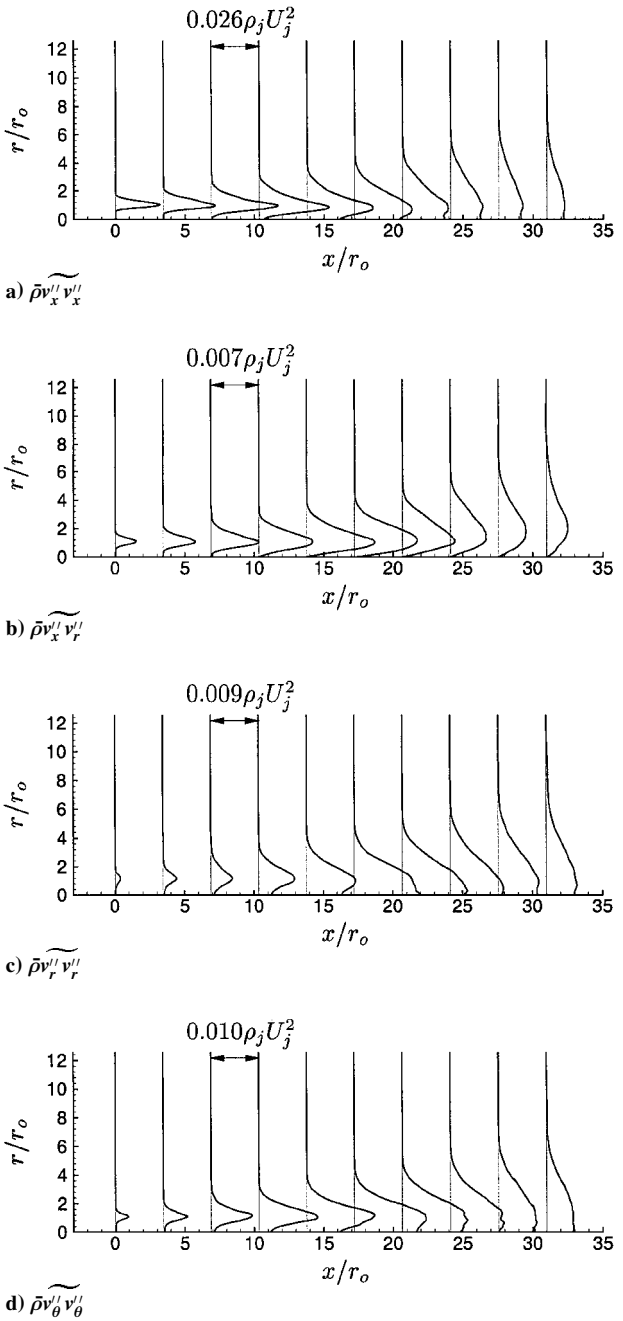

Fig. 5 Favre averaged Reynolds stresses.

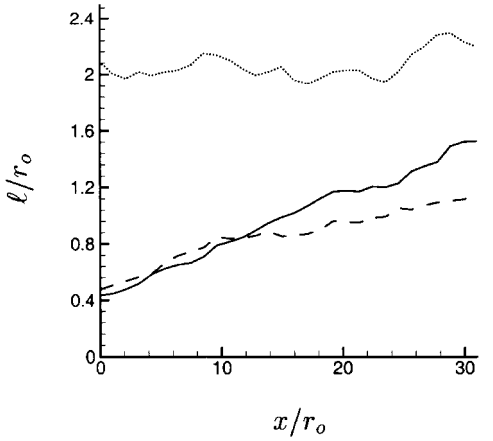

Fig. 6 Turbulence length scales at $r = r_o$: ——, radial; · · ·, axial; and – – –, azimuthal.

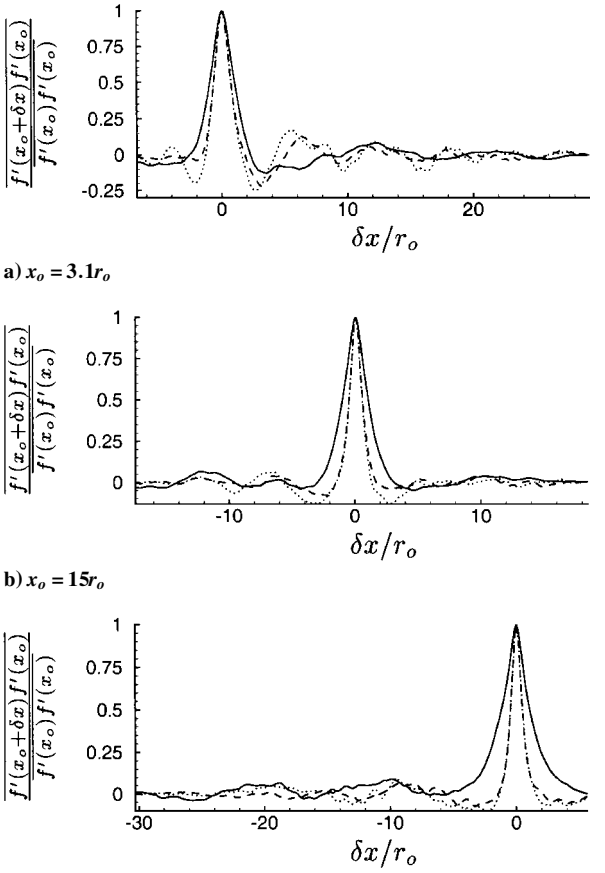

Fig. 7 Two-point velocity correlations in the x direction at $r = r_o$ with f representing: ——, u; – – –, v_r; and · · ·, v_θ.

then we define $\ell_x(x_o) = x_r + x_l$, where x_l and x_r are the distances from the correlation peak to the left and right 50% correlation points. The length scales in the other coordinate directions are defined similarly. Because the correlation length is a function of both x and r and because there is no self-similar scaling to collapse the data, the most relevant positions for presenting the data are not obvious. In the shear layer region, which appears to dominate the dynamics for most of the domain, the half-velocity point is an obvious choice. Plotted in Fig. 6 are ℓ_x, ℓ_r, and ℓ_θ at $r = r_o$, which approximates the half-velocity point before the potential core closes. The axial length scale remains constant $\ell_x \approx 2r_o$ over the entire axial extent of the domain. It is expected that farther downstream, where the jet will eventually show self-similar behavior, ℓ_x will also begin to rise. Not surprisingly, the radial correlation length increases linearly with downstream distance as the layer spreads. The azimuthal length scale also increases with downstream distance indicating that the turbulence becomes more azimuthally correlated at larger x. It is well known that mixing layers display higher spanwise or azimuthal correlations at lower Mach numbers, and so this behavior may be associated with a decreasing role of compressibility. However, it is also possible that this is simply due to the growth of the mixing region. The typical size of azimuthally and radially correlated structures may scale with a characteristic dimension of the jet or mixing region, such as the 99% velocity thickness, which also has approximately linear growth for the length of the computational domain. In the time developing simulations that were used to generate the inflow conditions, ℓ_x developed to be longer than ℓ_r and ℓ_θ. This is responsible for the observed length scales at $x = 0$.

The axial two-point velocity correlations are plotted in Fig. 7 for all three velocity components at three x locations. All correlations decay to a very small value away from the peak, which is typical of turbulent flows. If the dynamics were dominated by a single instability mode, we might expect a high-amplitude wavy streamwise correlation. Away from their peak at zero displacement, the correlations do decay in a wavy fashion, but the amplitudes are quite

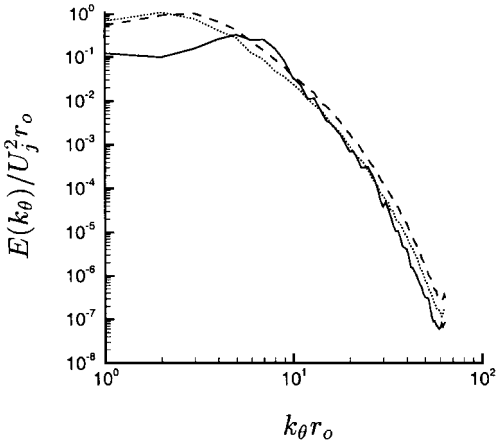

Fig. 8 One-dimensional azimuthal energy spectra at $r = r_o$; ——, $x = 0.1r_o$; – – –, $x = 12.6r_o$; and · · ·, $x = 18.7r_o$.

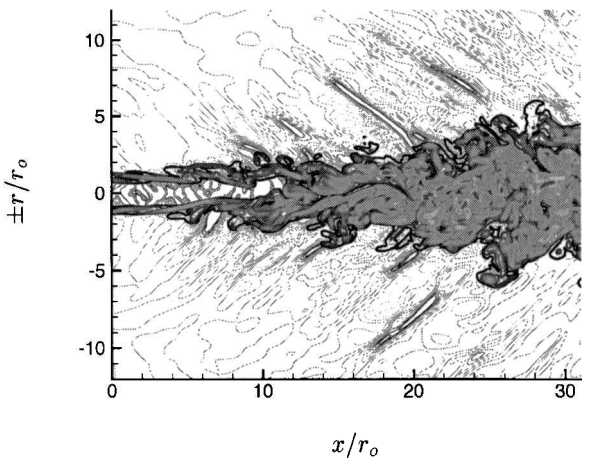

Fig. 9 Visualization of the jet and sound field; thick contours show vorticity magnitude with a maximum of $\omega_{max} = 10U_j/r_o$, and thin contours show dilatation between $\pm$ $0.025r_o/U_j$.

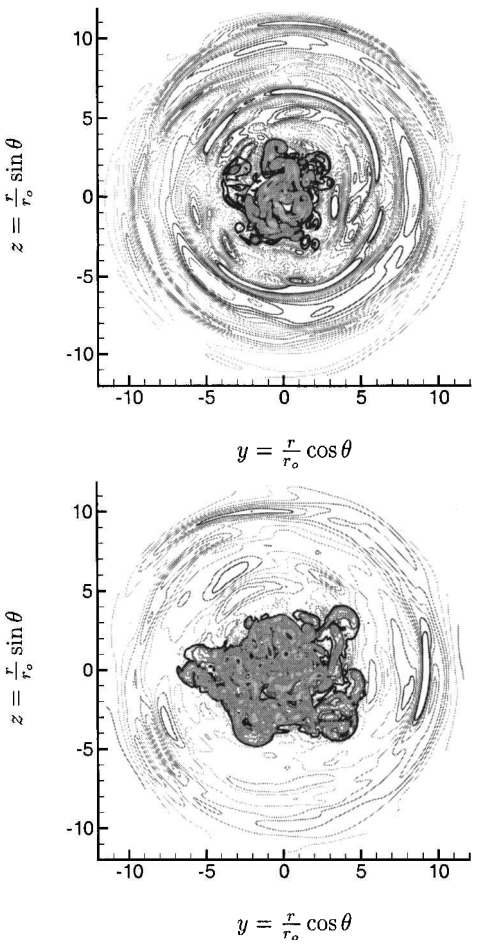

Fig. 10 Visualization of the jet and sound field; thick contours show vorticity magnitude with a maximum of $\omega_{max} = 10U_j/r_o$, and thin contours show dilatation between $\pm$ $0.025r_o/U_j$: top, $x = 15r_o$, and bottom, $x = 30r_o$.

low. The lack of a strong correlation does not necessarily imply that a linear mechanism is not at the root of the dynamics, at least in the shear layer region. A superposition of many randomly phased modes at similar but distinct or slowly varying streamwise wave numbers could also produce such a decorrelation.

D. Energy Spectra

It is important to test that simulated turbulence has a realistic broadbanded energy spectrum that decays rapidly at high wave numbers. Figure 8 shows the θ energy spectra at three different streamwise locations. The spectra are indeed broadbanded and decay significantly at higher wave numbers. The absence of an inertial range is a manifestation of the low Reynolds number of the present simulations. The shape of the high wave number end of the spectrum changes relatively little despite a large change in the low wave number spectral level and very different flow conditions at the various downstream locations.

IV. Acoustic Results

A. Visualization

The jet and its near acoustic field are visualized with vorticity and dilatation contours in Fig. 9. Vorticity marks the jet turbulence and decays rapidly into the acoustic field, which is by definition irrotational. Contours of dilatation in the near acoustic field reveal several steep compression waves. These are typical of the Mach waves observed in schlieren visualizations of supersonic jets. The Mach waves emanate from the end of the potential core, and all radiate away from the jet at nearly the same angle. This angle was estimated by assuming that the waves propagate normal to their apparent orientation in the visualizations. A sampling reveals that all distinct compressions have their normals between 45 and 55 deg off the jet axis. If we assume the waves are generated by a single source moving supersonically in the axial direction (while at fixed r and θ) and that the waves propagate at the sound speed, then, for a Mach angle of 50 deg, we estimate that this source is moving at a Mach number $U/a_\infty = 1.56$. This is somewhat lower than the jet Mach number 1.92 and roughly corresponds to the convection velocity of the dominant sound-producing turbulent eddies. However, one would need to account for flow acoustic interactions to identify the convection velocity from the Mach angle.

Views in r–θ planes show the Mach waves are highly three dimensional (Fig. 10). Regions of relatively intense compression typically span 90 deg in θ, but the waves appear to be correlated for longer azimuthal distances. The turbulence is also seen to be highly three dimensional. The azimuthal correlation of the Mach waves is also seen in Fig. 11, which shows the Mach waves on a cylinder at $r = 12r_o$ as they exit the physical portion of the computational domain.

B. Nonlinearities in the Acoustic Field

The primary concern with aircraft jet noise is what is heard on the ground, the far-field sound. To study this, it is necessary to calculate the sound further away from the jet than $r = 12r_o$. Several methods for doing this are reviewed by Shih et al.[12] These are classified into three categories: acoustic analogy, Kirchhoff methods, and direct methods. In the first, acoustic analogy, the flow equations are rearranged into assumed acoustic source terms and acoustic propagation terms and the resulting inhomogeneous wave equation is solved for the sound field. However, this approach is inappropriate in the present study where we intend to develop a database capable of evaluating acoustic theories and do not wish to rely on

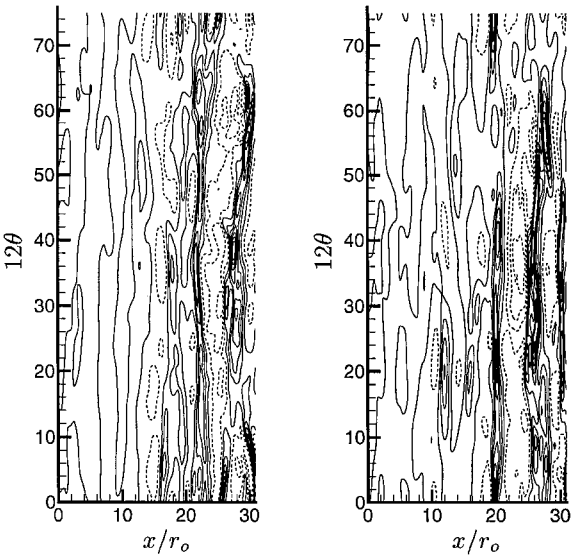

Fig. 11 Visualization of the Mach waves with dilatation contours on an unrolled cylinder at $r = 12r_o$; contours: $-0.04r_o/U_j$–$0.015r_o/U_j$, with positive contours dashed.

the assumptions made in the derivation and solution of analogies (see Ref. 13 for a critical analysis of acoustic analogies). Kirchhoff methods are often favored because they offer an analytically exact far-field linear acoustic solution given data on a surface enclosing all the sources. Even for open surfaces, which are required for jets, the errors can be quantified and somewhat corrected.[14] However, the formulation depends on Green's functions for the appropriate wave equation operator, and so, in cases where there are significant nonlinear acoustic effects, Kirchhoff methods are inappropriate. The final method, proposed by Freund et al.[15] and used by Shih et al.,[16] directly solves a simplified equation set into the far field. Both of these references proposed the linearized Euler equations as the acoustic field equation set, but extension to include nonlinear propagation effects is straightforward. For the present flow, which has clear nonlinear waves in the sound field, an analysis of nonlinear effects is needed before choosing a method.

Weak-shock theory[17] is a useful avenue for performing this evaluation. Lighthill[18] discusses a similar application of weak-shock theory to jet noise and Punekar et al.[19] have used Burgers equation solutions to study the statistical behavior of nonlinear random waves also with application to supersonic jet noise. A summary of the formulation used in this work, which is slightly different from the standard formulations, is provided in the Appendix.

Before applying this one-dimensional theory to test the validity of the linear approximation outside of the computational box, we will first test it against the Navier–Stokes solution for propagation of waves within the computational box. In particular, we need to test whether or not we can correctly estimate the propagation direction of the Mach waves and if omnidirectional turbulent mixing noise will hinder application of the one-dimensional theory. An initial condition is chosen on a ray inclined at 50 deg from the jet axis (Fig. 12a). Navier–Stokes, weak-shock, and linear theory ($\tau = t - s/a_\infty$) solutions are compared in Fig. 12b. By examining the linear and weak-shock solutions, one sees that nonlinear effects are not important for this short distance. The comparison with the Navier–Stokes solution is also favorable considering the possibility of three-dimensional effects and errors in estimating the Mach angle. These effects are blamed for the differences. The agreement is sufficient for estimation of nonlinear effects in the sound field.

At larger s, accumulated nonlinear effects are, of course, more significant. It can be seen in Fig. 13a that not far beyond the computational domain, which ends at $s \approx 19r_o$, the steepest wave starts to break. Notice, however, that the wave peaks predicted with the linear and nonlinear theories are not too dissimilar as far out as $s = 35r_o$ ($r = 27r_o$). This indicates that for a moderate extension of the sound field solution away from the Navier–Stokes domain, linear techniques should be able to correctly calculate sound pressure levels

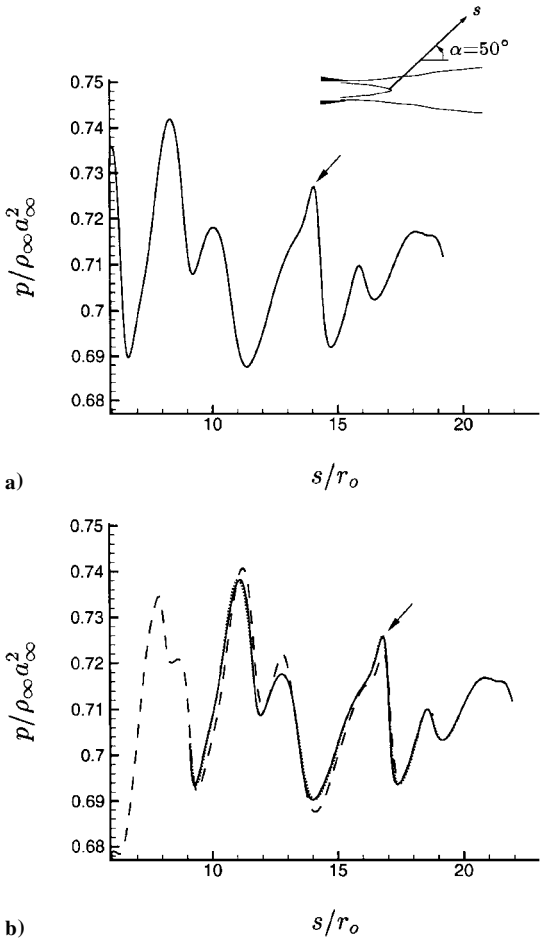

Fig. 12 Comparison of one-dimensional weak-shock theory for which arrows indicate a corresponding peak at the two times: a) initial condition at $t = t_o$ along a ray taken from the Navier–Stokes solution and b) at time $t = t_o + 2.7r_o/a_\infty$ calculated by – – –, Navier–Stokes; ——, weak-shock theory; and · · ·, linear theory.

and similar sound field statistics. However, important statistics that depend on the wave shapes, such as spectra, will be unreliable unless nonlinear effects are included. By $s = 80r_o$ ($r = 61r_o$) a distinct N-wave pattern develops in the pressure traces (Fig. 13b). We also see that some peaks predicted by nonlinear theory are significantly smaller than the corresponding linear predictions due to increased dissipation in the shocks. Thus, at large distances where a Kirchhoff method offers the greatest advantage over direct methods (for linear acoustics by avoiding the necessity of propagating the waves directly for a long distance) it will behave poorly because of its inherent linearity.

C. Extrapolation of the Acoustic Field

In the present study, no attempt was made to compare the flowfield to a particular jet experiment, all of which that would be appropriate were at Reynolds numbers too high to simulate directly. Also, there is typically insufficient documentation of near nozzle flow conditions in the available experimental results to specify precise inflow conditions to make a direct comparison. However, it is important to show that the overall sound pressure levels are within the range of those measured for jets at similar Mach numbers. Typically, experimental sound field data is measured starting at greater than 12 jet radii from the jet axis,[20–23] which is the extent of the Navier–Stokes domain in the present study. Therefore, to make a comparison it is necessary to extend the solution further from the Navier–Stokes computation into the sound field. Based on the results of the preceding section, a direct method for solving the Euler equations with shock fitting capability would be the most appropriate. However, it was also shown that a linear method should suffice for calculating the statistics of the acoustic field that do not depend heavily on the local wave shapes out to $r \approx 27r_o$. A linear wave equation solver, as

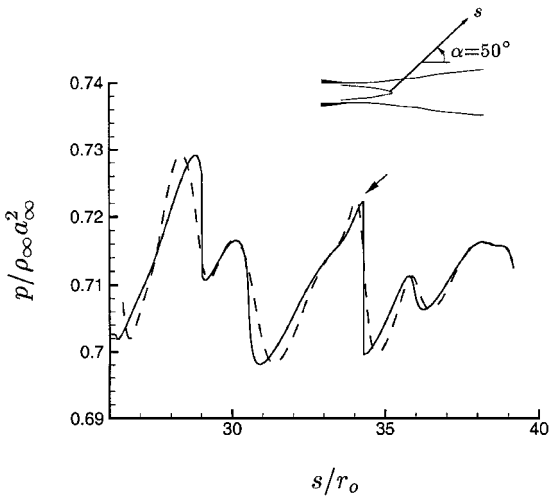

a) $t = t_o + 20r_o/a_\infty$

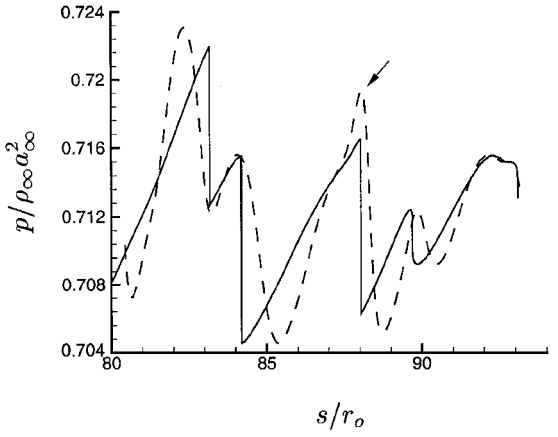

b) $t = t_o + 74r_o/a_\infty$

Fig. 13 Weak-shock theory vs linear theory for prediction of waveforms outside of the Navier–Stokes computational domain: ——, weak-shock theory, and – – –, linear theory for the following times.

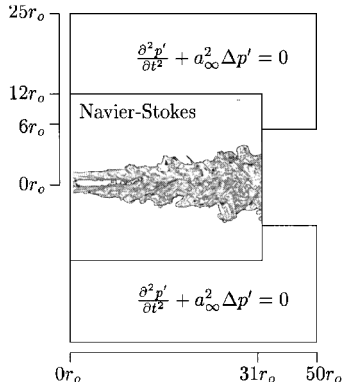

Fig. 14 Schematic showing the Navier–Stokes and coupled wave equation computational domains.

proposed by Freund et al.,[15] was used to propagate acoustic data from the Navier–Stokes solution out to $r = 25r_o$. A Kirchhoff method would also suffice for the present purpose, though it would not be exact because of the entrainment flow. The direct method was chosen because it is easier to implement and computationally cheaper for calculating time resolved data at every point in the extended domain.

The wave equation for the pressure fluctuations,

$$\frac{\partial^2 p'}{\partial t^2} + a_\infty^2 \Delta p' = 0 \tag{4}$$

where Δ is the Laplace operator in cylindrical coordinates, was solved numerically on the domain shown schematically in Fig. 14 using the same numerical algorithm as the Navier–Stokes solver. This domain was one-way coupled to the Navier–Stokes solver with a Dirichlet condition on p' applied on common boundaries. One-way coupling is not potentially as accurate as two-way coupling because an imperfect boundary condition must be applied on the inner solution[15]; however, tests showed that this was sufficiently accurate, and we shall see there is essentially no distortion of waves passing between the domains. A radiation boundary condition was applied on the other boundaries with the exception of the $r = 6r_o$ side where $p' = 0$ was enforced as a Dirichlet boundary condition. Ideally, pressure data from the downstream portion of the jet should be applied here, but due to the finite size of the Navier–Stokes domain, these data are not available. This is essentially the same problem that an open Kirchhoff surface poses[14] and may be analyzed in the same fashion. Essentially, an acoustically blocked region will not be physically realistic. For this reason, the region immediately above the $p' = 0$ boundary is not included in the analysis. The wave equation was discretized on a uniform mesh using $384 \times 150 \times 128$ mesh points in the axial, radial, and azimuthal directions. The mesh was rectangular but the points that overlapped the Navier–Stokes domain were not advanced in time. This wave equation computation was relatively inexpensive because the number of mesh points was small, the equation was very simple with few operations required per timestep, and significantly larger time steps could be taken because the grid was much coarser than in the jet flow. In addition, a significantly shorter run was needed because the sound field achieved a statistically steady state more rapidly than the Navier–Stokes solution. Overall, the wave equation computation required $< 1\%$ of the expense of the Navier–Stokes computation.

D. Acoustic Field Results

An instantaneous two-dimensional plane of the combined Navier–Stokes and wave equation solutions is shown in Fig. 15. No distortion of the waves passing between the two domains is discernible. Overall sound pressure levels (OASPL) were calculated for the acoustic field, and these are shown in Fig. 16. The acoustic radiation is highly directional, which is typical of jets at this Mach number.[20–23] However, if we compare peak OASPL levels at a given distance, the present jet is somewhat louder than other jets at similar Mach numbers. A table of peak OASPL at $r = 15r_o$ for the present study and several experiments is given in Table 1. The OASPL is 3 dB higher than the Troutt and McLaughlin[22] data at $M_j = 2.1$ and

Table 1 Peak overall sound pressure level at $r = 15r_o$ for various jets

Reference	M_j	Re	M_c	$\text{OASPL}_{\max}$, $r = 15r_o$
22	2.0	5.2×10^6	0.85	146 dB
23	2.1	7.0×10^4	0.86	151 dB
21	2.3	9.7×10^3	0.94	154 dB
Present	1.92	2.0×10^3	0.99	154 dB
24	2.5	8.7×10^3	1.00	156 dB

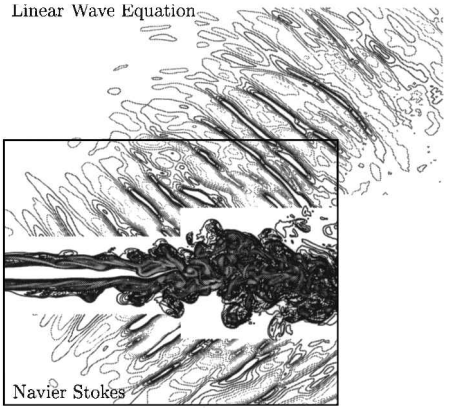

Fig. 15 Visualization of the combined Navier–Stokes and linear wave equation solution; the extended domain is shown only on the top, and the contours are similar to those of Fig. 9.

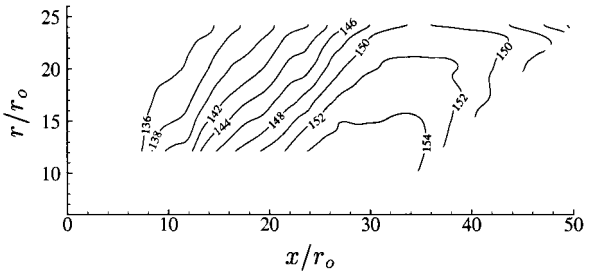

Fig. 16 Overall sound pressure levels in decibels.

8 dB higher than the Seiner and Ponton[21] data at $M_j = 2.0$. This is despite that the present jet is at a lower Mach number than either of these experiments. The difference may be explained by the choice of Mach number parameter. It is generally accepted that the mechanism for Mach wave radiation[3] (as well as growth of compressible mixing layers[24]) is strongly connected with the amplification rate of instability modes and that this scales with the convective number.[4] Before the potential core closes, a jet convective Mach number may be defined by

$$M_c = \frac{M_j\sqrt{T_j/T_\infty}}{1+\sqrt{T_j/T_\infty}} \tag{5}$$

By using Eq. (5), we essentially account for the present jet being nearly uniform in temperature, whereas the experiments under consideration have uniform stagnation temperatures. We see in Table 1 that the present jet at $M_c = 0.99$ agrees more closely with the jet of McLaughlin et al.[20] at $M_c = 0.94$ and the jet of Morrison and McLaughlin[23] at $M_c = 1.00$. More experimental data are necessary to properly test this scaling.

V. Conclusions

An $M_j = 1.92$ jet was simulated to provide simultaneous turbulent and sound field data. Mean flow profiles, Reynolds stresses, two-point correlations, and azimuthal energy spectra all demonstrate that the turbulence is realistic and that the statistical sample was sufficient to obtain converged statistics. Weak-shock theory established that nonlinear effects are important for calculation of the far-field sound, but also that linear methods suffice to estimate the near-field sound pressure levels. A linear wave equation was one-way coupled to the Navier–Stokes equation to calculate sound pressure levels outside the Navier–Stokes domain, and these were found to agree qualitatively with experiments. The results agreed best with jets at similar convective Mach numbers.

A future objective of this work is to test quantitatively the relation between the radiated sound and the linear stability modes in a turbulent supersonic jet. We want to determine whether a strong relation to the linear modes also exists in an unforced turbulent jet and to determine if there is indeed a linear relation between nozzle conditions and the sound field as suggested by the constant factor in the Tam and Burton[3] model. Such a relation is important for the development of systems models for jet noise prediction and control. Connection to the nozzle conditions is of particular interest because that is the most convenient place to implement a control strategy. Direct numerical simulation of a jet and its acoustic field will provide the full simultaneous flowfield information necessary for this analysis. Detailed processing of this current database from a jet noise prediction viewpoint is underway and will be reported in the future.

Appendix: Weak-Shock Theory

The weak-shock formulation used in this study is slightly different from others presented in the literature,[17,25] and, therefore, a brief outline of it is provided here. The analysis is motivated by the linearization of the gas dynamic equations not being uniformly valid for long range propagation of acoustic waves; the leading neglected term is secular. The first-order correction to this uses linear theory to describe the wave amplitudes, and so the conical Mach waves decay like $1/r^{1/2}$ away from the jet, but first-order nonlinear effects distort the wave profiles. A uniformly valid approximation results that can be used to study the propagation of finite amplitude waves.

The simulation data are most conveniently accessed as three-dimensional flowfields at an instant, and so it is convenient to formulate an initial value problem for data given at such an instant. We start from a characteristic solution of the form

$$\phi = f(\tau)/s^{\frac{1}{2}} \tag{A1}$$

where ϕ is a stream function, s is the distance along a characteristic curve, and τ parameterizes the initial data, $f(\tau)$. The $s^{1/2}$ term in Eq. (A1) is the geometrical factor appropriate for conical Mach waves. The pressure p, velocity parallel to the characteristic u_s, and sound speed a are

$$\frac{p-p_\infty}{p_\infty} = \frac{\gamma F(\tau)}{s^{\frac{1}{2}}} \tag{A2}$$

$$\frac{a-a_\infty}{a_\infty} = \frac{\gamma-1}{2}\frac{F(\tau)}{s^{\frac{1}{2}}} \tag{A3}$$

$$\frac{u_s}{a_\infty} = \frac{F(\tau)}{s^{\frac{1}{2}}} - \frac{1}{2}\frac{f(\tau)}{s^{\frac{3}{2}}a_\infty} \tag{A4}$$

where $F(\tau) = f'(\tau)$. The equation defining a characteristic is

$$\frac{\mathrm{d}t}{\mathrm{d}s} = \frac{1}{a+u_s} \quad \text{on} \quad \tau = \text{const} \tag{A5}$$

Neglecting perturbation terms of quadratic order and higher, this becomes

$$\frac{\mathrm{d}t}{\mathrm{d}s} = \frac{1}{a_\infty} - \frac{\gamma+1}{2}\frac{F(\tau)}{a_\infty s^{\frac{1}{2}}} + \frac{1}{2}\frac{f(\tau)}{a_\infty^2 s^{\frac{3}{2}}} \tag{A6}$$

We integrate this, neglect a term of $O(s^{-1/2})$, and set the integration constant to be τ to arrive at

$$\tau = t - s/a_\infty + (\gamma+1)[F(\tau)/a_\infty]s^{\frac{1}{2}} \tag{A7}$$

The solution procedure for initial data $p(s, t_o)$ given at discrete points on a ray (see Fig. 12 inset) is as follows. First Eq. (A2) is solved for $F(\tau)$ at each discretized initial condition point. Then Eq. (A7) is solved to calculate the appropriate τ for each of the initial data points. The solution at a later time $p(s, t_o + \Delta t)$ is then calculated by first solving Eq. (A7) for s in terms of known quantities $t = t_o + \Delta t$, $F(\tau)$, and τ, and then using Eq. (A2) to calculate the pressure. At large distances the solution can become multivalued. When this occurs, shocks are fitted assuming that the shock speed U_{shock} is the mean of the adjacent sound speeds, $U_{\text{shock}} = \frac{1}{2}(a_1 + a_2)$ (this is justified for weak shocks as a consequence of the Hugoniot law[25,26]). The well-known property that the net area between the fitted shock and the multivalued solution must be zero follows, and this uniquely positions the shock in a manner consistent with a weak formulation of the governing equations. Analytically it may be written[17]

$$\frac{1}{2}\{F(\tau_1)+F(\tau_2)\}(\tau_2-\tau_1) = \int_{\tau_1}^{\tau_2} F(\tau)\,\mathrm{d}\tau \tag{A8}$$

where the shock is fitted between characteristics τ_1 and τ_2.

Acknowledgments

These simulations were carried out while the first author was at Stanford University at the Center for Turbulence Research and funded by the Franklin P. and Caroline M. Johnson graduate fellowship. Computer time was provided by the Cornell Theory Center, the Corps of Engineers Waterways Experiment Station Major Shared Resource Center, the National Academy of Sciences, and NASA Ames Research Center.

References

[1]Tam, C. K. W., "Supersonic Jet Noise," *Annual Review of Fluid Mechanics*, Vol. 27, 1995, pp. 17–43.

[2]Tam, C. K. W., "Jet Noise Generated by Large-Scale Coherent Motion," *Aeroacoustics of Flight Vehicles*, edited by H. Hubbard, NASA RP-1258, Aug. 1991, pp. 311–390.

[3]Tam, C. K. W., and Burton, D. E., "Sound Generated by Instability Waves of Supersonic Flows. Part 2. Axisymmetric Jets," *Journal of Fluid Mechanics*, Vol. 138, Jan. 1984, pp. 273–295.

[4]Papamoschou, D., and Roshko, A., "The Compressible Turbulent Shear Layer: An Experimental Study," *Journal of Fluid Mechanics*, Vol. 197, Dec. 1988, pp. 453–477.

[5]Morris, P. J., "The Spatial Viscous Instability of Axisymmetric Jets," *Journal of Fluid Mechanics*, Vol. 77, No. 3, 1976, pp. 511–529.

[6]Mitchell, B. E., Lele, S. K., and Moin, P., "Direct Computation of the Sound Generated by Subsonic and Supersonic Axisymmetric Jets," Dept. of Mechanical Engineering, TR TF-66, Stanford Univ., Stanford, CA, Nov. 1995.

[7]Freund, J. B., Moin, P., and Lele, S. K., "Compressibility Effects in a Turbulent Annular Mixing Layer," Dept. of Mechanical Engineering, Flow Physics and Computation Div., TR TF-72, Stanford Univ., Stanford, CA, Sept. 1997.

[8]Freund, J. B., "Noise Sources in a Low Reynolds Number Turbulent Jet at Mach 0.9," *Journal of Fluid Mechanics* (submitted for publication).

[9]Freund, J. B., "A Proposed Inflow/Outflow Boundary Condition for Direct Computation of Aerodynamic Sound," *AIAA Journal*, Vol. 35, No. 4, 1997, pp. 740–742.

[10]Freund, J. B., Lele, S. K., and Moin, P., "Compressibility Effects in a Turbulent Annular Mixing Layer. Part 1. Turbulence and Growth Rate," *Journal of Fluid Mechanics*, Vol. 421, 2000, pp. 229–267.

[11]Crow, S. C., and Champagne, F. H., "Orderly Structure in Jet Turbulence," *Journal of Fluid Mechanics*, Vol. 48, No. 3, 1971, pp. 547–591.

[12]Shih, S. H., Hixon, D. R., Mankbadi, R. R., Pilon, P., and Lyrintzis, A., "Evaluation of Far-Field Jet Noise Prediction Methods," AIAA Paper 97-0282, 1997.

[13]Doak, P. E., "Analysis of Internally Generated Sound in Continuous Materials: 2. A Critical Review of the Conceptual Adequacy and Physical Scope of Existing Theories of Aerodynamic Noise, with Special Reference to Supersonic Jet Noise," *Journal of Sound and Vibration*, Vol. 25, No. 2, 1972, pp. 263–335.

[14]Freund, J. B., Lele, S. K., and Moin, P., "Calculation of the Radiated Sound Field Using an Open Kirchhoff Surface," *AIAA Journal*, Vol. 34, No. 5, 1996, pp. 909–916.

[15]Freund, J. B., Lele, S. K., and Moin, P., "Matching of Near/Far-Field Equation Sets for Direct Computation of Aerodynamic Sound," AIAA Paper 93-4326, 1993.

[16]Shih, S. H., Hixon, D. R., and Mankbadi, R. R., "A Zonal Approach for Prediction of Jet Noise," Confederation of European Aerospace Societies/AIAA Paper 95-144, 1995.

[17]Whitham, G. B., *Linear and Nonlinear Waves*, Wiley, New York, 1974, pp. 312–338.

[18]Lighthill, J., "Some Aspects of the Aeroacoustics of High-Speed Jets," Inst. for Computer Applications in Science and Engineering, 93-20, May 1993.

[19]Punekar, J. N., Ball, G. J., Lilley, G. M., and Morfey, C. L., "The Propagation and Bunching of Nonlinear Random Waves," Fifth International Congress on Sound and Vibration, International Inst. of Acoustics and Vibration, Dec. 1997.

[20]McLaughlin, D. K., Morrison, G. L., and Troutt, T. R., "Reynolds Number Dependence in Supersonic Jet Noise," *AIAA Journal*, Vol. 15, No. 4, 1977, pp. 526–532.

[21]Seiner, J. M., and Ponton, M. K., "Acoustic Data for High Reynolds Number Supersonic Axisymmetric Jets," NASA TM-86296, 1985.

[22]Troutt, T. R., and McLaughlin, D. K., "Experiments on the Flow and Acoustic Properties of a Moderate-Reynolds-Number Supersonic Jet," *Journal of Fluid Mechanics*, Vol. 116, March 1982, pp. 123–156.

[23]Morrison, G. L., and McLaughlin, D. K., "Noise Generation by Instabilities in Low Reynolds Number Supersonic Jets," *Journal of Sound and Vibration*, Vol. 65, No. 2, 1979, pp. 177–191.

[24]Morris, P. J., Giridharan, M. G., and Lilley, G. M., "On the Turbulent Mixing of Compressible Free Shear Layers," *Proceedings of the Royal Society of London, Series A: Mathematical and Physical Sciences*, Vol. 431, Jan. 1990, pp. 219–243.

[25]Lighthill, J., *Waves in Fluids*, Cambridge Univ. Press, Cambridge, England, U.K., 1974, pp. 165–175.

[26]Pierce, A. D., *Acoustics: An Introduction to Its Physical Principles and Applications*, Wiley, New York, 1974, pp. 574–586.

P. J. Morris
Associate Editor